LAWRENCE
LIVERMORE
NATIONAL
LABORATORY

LLNL-CONF-742568

Advanced multidomain method for multiphase flow interaction with Lagrangian structural meshes

Y. Kanarska, S. Schofield, T. Dunn, B. Liu, C. Noble

November 30, 2017

MULTIMAT
Santa Fe, NM, United States
September 18, 2017 through September 22, 2017

Disclaimer

Advanced multi-domain method for multiphase flow interaction with Lagrangian structural meshes

Yuliya Kanarska[1], Samuel Schofield, Timothy Dunn, Benjamin Liu, Charles Noble
Lawrence Livermore National Laboratory
[1]kanarska1@llnl.gov

Keywords: embedded grids, interface, multiphase flow, Lagrange hydro

ABSTRACT

Multiphase flow with particulates has emerged as a topic of fundamental fluid and continuum mechanics interest in many applications including national security applications. For more efficient simulation workflows, the utilization of a separate background multiphase flow mesh and foreground Lagrangian structural meshes is greatly beneficial. We propose a multi-domain coupling method for multiphase Godunov compressible high-speed flow interacting with an ALE structure on a different mesh. Along with cell centered updates in ghost points similar to ghost fluid methods we use additional modifications of the solid states at faces in such a way that resulting solution of the Riemann problem at each face satisfies the boundary interface conditions. Due to variation in targets and potentially dense particulate phases, the embedded grid coupling methodology needs to be stable across a wide range of fluid/structure density ratios as well as both dense and dilute particle regimes. We are developing multiphase extensions of the Banks, et. al. (2011) interface conditions that are appropriate for the wide range of multi-phase flow conditions. Several examples demonstrate applicability of the method for multiphase flow interaction with dynamic deformable Lagrangian structural meshes.

1. Introduction

In the research community, there has been significant progress in numerical methods for fluid-structure interaction with high speed flows (Pember aet al., 1995, Peskin et al., 2002, Ghias et al., 2007, Tipton et al. 2011, Puso et al., 2012). However, little work has been done on the consistent

coupling of multiphase compressible flow with Lagrange structural meshes. To provide a more productive capability with rapid analysis turnaround, the utilization of separate background multiphase flow meshes and foreground Lagrangian structural meshes is greatly beneficial. A solid model used for structural or thermo-mechanical calculations can be used almost "as is" in the dynamic calculation. These targets often have very unstructured meshes making the creation of a globally conformal mesh that ties the structure to the finely, reasonably uniform, zoned mesh required for the turbulent high-speed flow calculation extremely challenging. The embedded mesh approach has much more flexibility and is clearly preferred, however, there are significant challenges in extending the numerical methods used for embedded boundaries to multiphase formulations that are currently used for multiphase blast. There has been significant progress in numerical methods for fluid-structure interaction with high speed flows including the ghost fluid method (Fedkiw, 2002, Ghias 2007, Tipton et al., 2011), cut cell method (Pember et al., 1998), immersed boundary method (Peskin, 2002), Lagrange multiplier method (Pusso et al., 2012). The primary difficulty of standard embedded grid schemes is that traditional discrete interface conditions often result in numerical instability. Due to variation in target and potentially dense particulate phases, the embedded grid coupling methodology needs to be stable across a wide range of fluid/structure density ratios, something only few coupling methods have (Banks et al., 2011).

The proposed approach is the extension of the ghost fluid method to couple Eulerian multiphase to ALE Lagrangian solid dynamics including interaction of multiphase particles with the foreground mesh. We have combined a number of ideas from the recent literature including ghost-fluid and embedded interface methods. Some unique features of this work include development of a multiphase (and even multiple EOS) extension of the Banks, et. al. (2011) interface conditions that is appropriate to couple multiphase fluid with Lagrangian structures across wide range of material properties. In addition to the ghost cell updates we modify the left and right Riemann states similar to Gorsse et al., (2011) in such a way that resulting solution of the Riemann problem at each face satisfies the boundary interface conditions. These modifications allow achieving higher accuracy of the resulting scheme.

The paper is organized as follows: In section 2 a short description of our multi-domain approach is presented. The multiphase solver equations and algorithm are briefly described in section 3. The low Mach number corrections to the standard compressible flows are presented in section 4.

Section 5 outlines the explicit Lagrangian hydrodynamic equations and solver. The mesh intersection and element categorization is described in Section 6. The interface conditions used are detailed in section 7 and the coupling technique is described in section 8. Verification, validation, and numerical simulations are discussed in section 9. Conclusions and future work are given in the last section.

2. Multi-domain partitioned approach

ALE3D code is a multi-physics numerical simulation software tool utilizing arbitrary-Lagrangian-Eulerian (ALE) techniques (Noble et al., 2017). It has different physical solvers and mesh generation techniques. The goal of our multi-domain multi-physics coupling approach is to couple different solvers in ALE3D that operate on different domains and meshes. However, the technique described in this paper can be adopted for other multiphysics codes as well. Each domain and its associated simulation solver and mesh are isolated and communicate with other domains only through surfaces. A problem can be decomposed into domains on which an appropriate solver is chosen, for instance a rigid body solver coupled with an explicit time stepping compressible flow solver or a thermal-mechanical solid model can be coupled with an incompressible flow model. This approach is often referred to as “partitioned” and has many advantages including low memory requirements, low computational cost, and high parallel efficiency. There is no need to solve globally coupled systems of equations, which can be problematic particularly during parallel execution. Since the coupling occurs only through surfaces, well tested single physics solvers can be used, with each solver remaining separate and operating on its own domain. This will also enable different fluid and/or solid solvers to be exchanged with minimal effort. In a numerical scheme, there are many ways that velocity- and stress-continuity can be enforced in the discrete approximation. Banks et al., (2011) performed a normal mode stability analysis of the linearized problem to investigate the stability of different numerical interface conditions for a model problem approximated by upwind type finite difference schemes. Their analysis shows that depending on the ratio of densities between the solid and the fluid, some numerical interface conditions are stable up to the maximal Courant–Friedrich–Levy (CFL)-limit, while other numerical interface conditions suffer from a severe reduction of the stable CFL-limit. They also proposed a new interface condition which is

obtained as a simplified characteristic boundary condition (described in Section 7), that is proved to not suffer from any reduction of the stable CFL-limit.

In this paper, we are extending and applying these conditions for coupling multiphase fluid with Lagrange structures. We describe the coupling technique with application to the finite volume multiphase solver described in section 3 and finite element Lagrange hydro solver described in section 4.

3. Multiphase flow equations

The multiphase solver is based on the finite volume method using the discrete equation model (DEM) and allows description of multiple multiphase species, including dense particles (Chinnaya et al., 2003, Dunn, 2011). In this model, each phase has its own velocity and thermodynamic state (pressure, temperature, etc.). The presence of multiple velocities requires a modification to the standard single-phase ALE integration. The multiphase model handles these complications by integrating discrete equations for volume fraction α (can vary between 0 and 1), density ρ, momentum ρu, and total energy ρE of each species. Considering two-phase gas-particle flow, this model is described by a system of seven partial differential equations: conservations of mass, momentum, and energy for each phase, plus an additional equation for the evolution of volume fraction. For one-dimensional flow, these equations are given as:

$$\frac{\partial \alpha_c}{\partial t} = -V^I \frac{\partial \alpha_c}{\partial x} \tag{1}$$

$$\frac{\partial \alpha_c \rho_c}{\partial t} + \frac{\partial \alpha_c \rho_c u_c}{\partial x} = 0 \tag{2}$$

$$\frac{\partial \alpha_c \rho_c u_c}{\partial t} + \frac{\partial (\alpha_c \rho_c u_c^2 + \alpha_c P_c)}{\partial x} = P^I \frac{\partial \alpha_c}{\partial x} + F^I \tag{3}$$

$$\frac{\partial \alpha_c \rho_c E_c}{\partial t} + \frac{\partial (\alpha_c \rho_c u_c E_c + \alpha_c u_c P_c)}{\partial x} = P^I V^I \frac{\partial \alpha_c}{\partial x} + F^I V^I + Q^I \tag{4}$$

$$\frac{\partial \alpha_d}{\partial t} = V^I \frac{\partial \alpha_c}{\partial x} \tag{5}$$

$$\frac{\partial \alpha_d \rho_d}{\partial t} + \frac{\partial \alpha_d \rho_d u_d}{\partial x} = 0 \tag{6}$$

$$\frac{\partial \alpha_d \rho_d u_d}{\partial t} + \frac{\partial (\alpha_d \rho_d u_d^2 + \alpha_d P_d)}{\partial x} = -P^I \frac{\partial \alpha_c}{\partial x} - F^I \tag{7}$$

$$\frac{\partial \alpha_d \rho_d E_d}{\partial t} + \frac{\partial (\alpha_d \rho_d u_d E_d + \alpha_d u_d P_d)}{\partial x} = -P^I V^I \frac{\partial \alpha_c}{\partial x} - F^I V^I - Q^I \tag{8}$$

where the subscripts *c* and *d* indicate properties of the carrier phase or discrete particle phase respectively. For simplicity we present 1D equations, whereas the numerical code operates on 3D grids. Details of the model equations and solution can be found in Saurel & Abgrall (1999) and Dunn (2011). The left sides of the equations represent the hydrodynamic response of the material, whereas the right-hand-side represents the non-conservative interaction between phases. These non-conservative terms account for momentum and energy transfer from one phase to the other due to various mechanisms such as drag F^I and heat transfer Q^I. The equations are solved indirectly using the Discrete Equation Method (DEM) of Chinnayya et al. (2004). The key idea is to discretize the multiphase mixture at the microscopic level and then to average the discrete equations. It provides a new discrete model as well as the numerical method. The DEM implicitly defines the values for the interface pressure P^I and interface velocity V^I and evaluation of these terms can be found in Chinnaya et al. (2004) and Dunn (2011). The resulting DEM equations are discretized using an Eulerian-based Godunov finite volume method with mesh motion. The convective and mesh motion integral terms are evaluated as surface fluxes. The DEM prescribes that these fluxes are computed at each inter-phase contact as well as contacts between different phases. The current formulation uses the Artificial Upstream Flux vector Splitting (AUFS) scheme of Sun & Takayama (2003) by default to compute the flux. It should be noted, that the numerical method presented here can be applied to any finite volume multiphase solver, but DEM method is chosen here since it has already existed in ALE3D code.

4. Low Mach correction.

It is known that low Mach features are heavily dampened in the standard compressible numerical schemes. Venkatesewaran and Merkle (1998) and Thornber et al. (2008a) demonstrated that the leading order kinetic energy dissipation rate in a finite volume Godunov scheme increases as Mach number *M* decreases. In the particular case of the MUSCL advection scheme with a van Leer limiter it was shown that the leading order kinetic energy dissipation rate can be written as

$$\epsilon = \frac{\Delta x^2}{12} u u_x u_{xx} + \frac{\Delta x^3}{24}(3u_{xx}^2 + (2C-3)u_x u_{xxx}) \quad (9)$$

where u and a are the velocity normal to the cell interface and speed of sound, respectively, C is the Courant–Friedrich–Levy (CFL) number and Δx is the cell length. Therefore, the dissipation is proportional to the speed of sound and the magnitude of the velocity derivatives squared at leading order. It was demonstrated that the increase in dissipation at low Mach numbers is not physical, but is a property of the discrete system. Thornber et al., (2008) proposed a simple modification of the reconstruction process within finite volume schemes to allow significantly improved resolution of low Mach number perturbations for use in mixed compressible/incompressible flows. The idea of the method is to modify left u_L and right states u_R computed using standard compressible solver as

$$u_{LM,L} = \frac{u_L+u_R}{2} + z\frac{u_L-u_R}{2} \quad (10)$$

$$u_{LM,R} = \frac{u_L+u_R}{2} + z\frac{u_R-u_L}{2} \quad (11)$$

where $z = \min(M_{local}, 1)$ and $M_{local} = \max(M_L, M_R)$.

We implemented this correction in the DEM multiphase solver. It will be shown in example 9.1 in Section 9 that such modifications prevent the numerical suppression of low Mach number flow instabilities.

5. Lagrangian hydrodynamic equations

The arbitrary Lagrangian-Eulerian hydrodynamic solver solves the equations of motion in the Lagrange frame and accomplishes advection numerically by calculating fluxes between the Lagrange mesh and its relaxed or Eulerian mesh. Compressible flow modeling is accomplished via the addition of an artificial viscosity term to the momentum equation. The equations of motion and the energy equation are discretized using the finite element method

The momentum equations are

$$\frac{\partial \sigma_{\alpha\beta}}{\partial x_\beta} + \rho f_\alpha = \rho \ddot{x}_\alpha \quad (12)$$

where $\sigma_{\alpha\beta}$ is the Cauchy stress, ρ is the density, and f is the body force density and x_α is the displacement.

Mass conservation is stated as

$$\rho V = \rho_0 \quad (13)$$

where V is the relative volume and ρ_0 is the reference density.

The energy equation is

$$\dot{E} = V s_{\alpha\beta} \dot{\epsilon}_{\alpha\beta} - (p+q)\dot{V} \quad (14)$$

which is integrated in time and used for the equation-of-state (EOS) evaluations and a global energy balance. The deviatoric stresses are

$$s_{\alpha\beta} = \sigma_{\alpha\beta} - (p+q)\,\delta_{\alpha\beta} \quad (15)$$

where p is pressure and defined as

$$p = -\frac{1}{3}\sigma_{\lambda\lambda} - q \quad (16)$$

q is the artificial viscosity, $\delta_{\alpha\beta}$ is the Kronecker delta, and $\dot{\epsilon}_{\alpha\beta}$ is the strain rate tensor. As most hydrocodes, we split the stress into the pressure which comes from the EOS and the deviatoric stress which is obtained in an incremental form using the Jaumann rate and a traditional Wilkins type plasticity treatment. Details of the numerical solution procedure can be found in Noble et al., (2017).

6. Mesh intersection and element categorization

At each cycle, the intersection of the exterior boundary of the foreground mesh with the background mesh is computed. The result of the calculation is a set of interface segments, which are portions of the exterior faces of the foreground mesh clipped to the background mesh cell in which they are contained. For each segment the outward normal, segment center, and segment area are computed and stored (Figure 2). For efficient identification of ghost cells of the background grid, underlying the foreground mesh and its boundary, a distance function φ is used. The signed distance to the interface segment is evaluated at each node of the element φ_N and at the element center φ_C. Based on those signed distances, the elements are categorized as fluid (all $\varphi_N > 0$ and t $\varphi_C > 0$), fluid-cut (some $\varphi_N < 0$ and $\varphi_C > 0$), solid-cut (some $\varphi_N < 0$ and $\varphi_C < 0$), and ghost (all $\varphi_N < 0$ and $\varphi_C < 0$) elements. For categorization, the foreground is deemed to be the "solid" and the background the "fluid", although properly the foreground ALE solver can also be fluid, that is materials without strength. Element categorization according to the signed distance is presented in Table 1. An example for a circular interface is shown in Figure 3. The element categorizations are used to update solution. The fluid-cut cells are treated as any other cells in the multiphase solver. Fluid-cut and fluid elements are used to

enforce boundary conditions at the interface. The solutions for ghost and solid-cut elements are updated using specified interface conditions. In addition, the element categorization is used to define which fluxes at the faces need to be modified. It will be shown in section 8 that in addition to the cell-center update, similar to the most ghost fluid methods, we modify the solid side of the Riemann problem at the faces which result in better accuracy of the coupling scheme.

Table 1. Element categorization according to the signed distance.

φ_C	φ_N	Element category	Description
$\varphi_C > 0$	All $\varphi_N > 0$	Fluid	Element outside the interface
$\varphi_C > 0$	Some $\varphi_N < 0$	Fluid-cut	Element cut by interface
$\varphi_C < 0$	Some $\varphi_N < 0$	Solid-cut	Element cut by interface
$\varphi_C < 0$	All $\varphi_N < 0$	Ghost	Element inside the interface

7. Interface conditions

Standard fluid structure interaction (FSI) conditions are usually formulated as follows: (1) the fluid velocity is forced to be equal to the solid velocity and (2) solid boundary conditions include pressure boundary conditions taken from the fluid. However, Banks et al. (2011) showed that such approximation may lead to numerical instabilities if the solid and fluid have similar densities, which could be the case of multiphase dense particles. In the recent articles (Banks et al., 2011 and Banks et al., 2014), a stable interface projection scheme was developed for the problem of coupling a compressible and incompressible fluid with stress and velocity state $(\boldsymbol{\sigma_L}, \boldsymbol{u_L})$ and a deformable elastic solid states $(\boldsymbol{\sigma_R}, \boldsymbol{u_R})$ of arbitrary density ρ_L and ρ_R. These conditions can be summarized as

$$\boldsymbol{n^T u_I} = \frac{\epsilon_L}{\epsilon_R+\epsilon_L}\boldsymbol{n^T u_R} + \frac{\epsilon_R}{\epsilon_R+\epsilon_L}\boldsymbol{n^T u_L} + \frac{1}{\epsilon_R+\epsilon_L}\boldsymbol{n^T}(\boldsymbol{\sigma_R n} - \boldsymbol{\sigma_L n}), \tag{17}$$

$$\boldsymbol{t^T u_I} = \frac{\epsilon_L}{\epsilon_R+\epsilon_L}\boldsymbol{t^T u_R} + \frac{\epsilon_R}{\epsilon_R+\epsilon_L}\boldsymbol{t^T u_L} + \frac{1}{\epsilon_R+\epsilon_L}\boldsymbol{t^T}(\boldsymbol{\sigma_R n} - \boldsymbol{\sigma_L n}), \tag{18}$$

$$\boldsymbol{n^T \sigma_I n} = \frac{\epsilon_L}{\epsilon_R+\epsilon_L}\boldsymbol{n^T \sigma_L n} + \frac{\epsilon_R}{\epsilon_R+\epsilon_L}\boldsymbol{n^T \sigma_R n} + \frac{1}{\epsilon_R+\epsilon_L}\boldsymbol{n^T}(\boldsymbol{u_R} - \boldsymbol{u_L}), \tag{19}$$

$$\boldsymbol{t^T \sigma_I n} = \frac{\epsilon_L}{\epsilon_R+\epsilon_L}\boldsymbol{t^T \sigma_L n} + \frac{\epsilon_R}{\epsilon_R+\epsilon_L}\boldsymbol{t^T \sigma_R n} + \frac{1}{\epsilon_R+\epsilon_L}\boldsymbol{t^T}(\boldsymbol{u_R} - \boldsymbol{u_L}), \tag{20}$$

where impedances are $\epsilon_{L,R} = 1/c\rho_{L,R}$, $\boldsymbol{n}$ is a unit normal to the interface and $\boldsymbol{t}$ is the outward vector tangent to the interface (there are two tangential mutually orthogonal vectors in 3D). It was shown by Banks et al., (2011) that the last term in these equations can be dropped because they are approximations to the interface coupling conditions of no jump in stress or velocity. Also, they mention that they could be kept if one desired. Such conditions proved to be stable for the entire range fluid/solid density ratios including the difficult regime of light solids coupled to heavy fluids. Such a stable coupling has been elusive in the literature and lays the groundwork for other coupling regimes. We used such conditions to develop a coupling scheme for each pair of multiphase variables and Lagrange hydro variables. Those averaged values are later extrapolated to both multiphase solver and Lagrange hydro as shown in the next section.

8. Coupling scheme

In this section, the numerical algorithm of solving the multiphase equations and Lagrange hydro equations on the coupled meshes is presented. The numerical solution is derived as multi-stage procedure illustrated in Figure 4 as follows

Step1: Advance Lagrange hydro

Solve the ALE Lagrange hydro equations to advance the solution from time step *n* to *n+1*. The interface pressure and velocity computed at the end of previous time step are applied as the boundary conditions to the Lagrange mesh. There are several options for the averaging techniques to derive the interface pressure. The first option is to use volume averaging of the pressures for each species at the interface. The second option is to use impedance averaging of the species pressures. We are currently using the first option of averaging in this paper and will consider other options later on. Once the averaged pressure is available the solution is advanced using the standard Lagrange hydro approach described in Section 3.

Step 2: Define interface conditions

We update the interface position at time step *n+1,* create interface segments and categorize elements. We calculate interface conditions at the mesh interface at *n+1* time step for each state variable. For each segment, we find the closest fluid and solid elements and derive interface

conditions in the projection to normal. We use impedance-weighted conditions described in Section 7. In the case of the frictionless compressible flow and slip boundary conditions between solid and multiphase we use those interface conditions for hydrodynamic pressure p. As suggested by Banks et al. (2011) we also dropped last terms. Each multiphase species has its own interface conditions (p_I^i, u_I^i) based on the impedance averaging of species state (p_m^i, u_m^i) and Lagrange hydro material (p_l, u_l) as

$$p_I^i = \frac{\epsilon_l p_l + \epsilon_m^i p_m^i}{\epsilon_m^i + \epsilon_l} \tag{21}$$

$$u_I^i = \frac{\epsilon_l u_m^i + \epsilon_m^i u_l}{\epsilon_m^i + \epsilon_l} \tag{22}$$

This interface values are used to update multiphase variables in ghost and solid-cut regions as described at the next steps.

Step 3: First order ghost update

Since ghost zones can be uncovered at the next time step due to the mesh motion we need to update those values. We use first order neighbors and interface values derived at Step 2. First, we project a ghost fluid grid point of interest onto the fluid–structure interface and determine its reflection (image point) with respect to the interface segment containing that ghost fluid grid point (cell 0 in Figure 4, Step 3). Since an image point usually falls in the physical fluid domain, the fluid state variables at this point are computed by interpolation, using available first order neighbors (cells 1, 2 and 3 in Figure 4, Step 3). Then, the multiphase velocity state vector for each species at the ghost fluid grid point is computed as follows. The fluid velocity vector (or its normal component in the case of slip boundary conditions) is obtained by linearly extrapolating the interpolated fluid velocity vector at the image point and the structural velocity vector at the projection point. The values of the remaining primary fluid variables (mass, pressure, internal energy and volume fractions) at the ghost fluid grid point are set to the interpolated values at the image fluid grid point. This step is somewhat similar to the ghost fluid methods (e.g. Ghias et al., 2007). However, to improve accuracy of the method, additional modifications to the face variables are done at the Step 5. This step is also necessary in the case of moving objects. When a cell changes from a ghost cell to a fluid cell, ghost values become a fluid and further evolved as any other fluid data.

Step 4: Find states of the Riemann problem in multiphase solver

At this step, we find the left and right states of the Riemann problem for multiphase fluid variables using standard MUSCL reconstruction scheme for each multiphase species as $U_+ = (\alpha_+, \rho_+, u_+, p_+)$ and $U_- = (\alpha_-, \rho_-, u_-, p_-)$. We will further assume that the solid side corresponds to U_+ and fluid side corresponds to U_-.

Step 5: Second order interface update

Extrapolate interface conditions defined at Step 2 to the faces using first and second order neighbor elements (Figure 4). We update here the face states for the cell 0 (see Step 5 in Figure 4). In particular, the value of u_* is determined by the following formula

$$(\boldsymbol{u}_* \cdot \boldsymbol{n_I}) = (\boldsymbol{u_I} \cdot \boldsymbol{n_I}) + (\tfrac{1}{2} - d)s \tag{23}$$

$$(\boldsymbol{u}_* \cdot \boldsymbol{\tau_I}) = (\boldsymbol{u}_- \cdot \boldsymbol{\tau_I}) \tag{24}$$

where d is the distance between interface point I and cell center 1 (Step 5 in Figure 4). Interface point I is evaluated as the intersection of the boundary of the foreground grid with the line connecting the cell centers 0 and 1 (Step 5 in Figure 4). Slope s for velocity field is computed using d-weighted slope computation as in Gorsse et al., (2012) as

$$s = \boldsymbol{u_I} \cdot \boldsymbol{n_I} - \boldsymbol{u_1} \cdot \boldsymbol{n_I} + \tfrac{1-d}{1+d}(\boldsymbol{u_I} \cdot \boldsymbol{n_I} - \boldsymbol{u_2} \cdot \boldsymbol{n_I}), \tag{25}$$

where $\boldsymbol{u_I}$ is the interface velocity computed at the previous step, $\boldsymbol{u_1}$ is the velocity of the cell 1 and $\boldsymbol{u_2}$ is the velocity of the cell 2 (Step 5 in Figure 4). Computing slope in this way allows avoiding instability when the cell center 1 is close to the interface I. If the slope limiter is needed the limiter slope is defined as $s_{limiter} = minmod(s, s_2)$, where

$$s_2 = \boldsymbol{u_1} \cdot \boldsymbol{n_I} - \boldsymbol{u_2} \cdot \boldsymbol{n_I} \tag{26}$$

Interface pressure is assumed to be equal to the interface pressure computed at the previous step as $p_* = p^I$. As a result of this procedure we will have interpolated interface values (u_*, p_*) to be used at the next step.

Step 6: Modify Riemann states

At this step, we modify the solid side of the Riemann problem for each multiphase species using extrapolated face interface values defined at the previous step as $U_+ = (\alpha_-, \rho_-, -u_- + 2u_*, p_*)$

Modified in this way the solution of Riemann problem at the faces satisfies exactly the boundary interface conditions at the faces. With states on either side of the interface in this way, the exact solution to the Riemann problem is symmetric about the path of the interface in *x-t* plane. When velocity of the fluid side state u_- is less than interface velocity u_*, the solution consists of two rarefactions. When velocity the fluid side state u_- is greater than the interface velocity u_*, the solution consists of two shock waves.

Step 7: Advance multiphase solution

The Artificially Upstream Flux-vector Splitting (AUFS) (Sun and Takayama, JCP, 2003) Riemann solver is used to advance the solution on the background multiphase flow mesh. This step completes the coupling scheme at time n+1.

9. Numerical results

In this section, we demonstrate the effectiveness of the presented coupling method for dynamic Lagrange hydro interfaces and their interaction with multiphase fluid across the entire range of material parameters for both single and multiple phases. All gases in the considered problem are modeled as ideal gases with adiabatic exponent $\gamma = 1.4$. Since the multiphase solver is explicit we use CFL number 0.4 in all examples.

9.1 Low Mach example

In this example, we demonstrate applicability of the underlying multiphase flow for subsonic flow applications. In this case, an initial subsonic flow that moves from the left to right with Mach number 0.05 interacts with a step-like structure (Figure 5). We did simulations with an original compressible scheme for multiphase flow and modified scheme with the Low Mach correction described in Section 4. We used a 2D configuration with 640 by 320 mesh resolution. The vorticity field in both simulations is presented in Figure 5. We can see that the original scheme heavily damps the Low Mach instabilities at the interfaces. The low Mach correction reduces the dissipation allowing the scheme to capture the interfacial instabilities.

9.2 Advection with uniform velocity

Here we present a test when the solid object moves diagonally with the same velocity as the surrounding fluid. In this case, there should be no artificial flows generated if the interface conditions and ghosts, fluid-cut and solid-cut elements are updated correctly. Mesh resolution was 13x13. Figure 6 shows the initial velocity and the velocity after 200 cycles. It is unchanged and there is no artificial flow generated. Therefore, we conclude that the method proposed in this paper has been implemented correctly.

9.3 Piston problem

The initial problem consists of a gamma law gas on the left and right and a solid piston in the center. The problem setup is similar to what was used in Dunn et al., (2011). Initially, the gas on the left is at a higher pressure than the gas on the right, resulting in a pressure force pushing the piston to the right. As the piston moves, the volume on the left increases causing a decrease in the pressure on the left. At the same time, the volume on the right decreases causing an increase in the pressure on the right. Eventually, the pressure on the right becomes greater than the pressure on the left causing the piston to decelerate and then get pushed to the left. Thus, the pressure force causes the piston to travel back and forth in a cyclic fashion. The initial geometry for this problem is shown in Figure 7. We used a 3D configuration with 40x8x8 mesh resolution. The problem consists of a rigid piston separating two gases. The piston is modeled using properties similar to steel, resulting in an essentially rigid material. This problem uses a one-dimensional geometry. It is modeled using a two-dimensional mesh with a single zone in the y direction and symmetry boundary conditions on the sides, resulting in a pseudo-1D flow in the x direction. The problem has a domain length of 4 with the origin (x = 0) at the center. The piston's length is 1. Initially, the gas on the left has a length of 1 and the right gas has a length of 2. Thus, the initial volume of the gas on the right is twice the volume of the gas on the left. Therefore, the pressure in the left gas is initially twice that of the right gas.

We did several simulations by varying piston/gas density ratios and used a standard FSI coupling conditions and impedance averaged interface conditions presented in Section 7. Figure 7 shows the results of simulation for 100 piston/air mass ratio and 0.01 piston/air ratio. In the last case the

piston was simulated as a low density fluid. Figure 7c shows that the spurious waves are generated for a piston problem without impedance conditions at low solid/fluid density ratios, whereas the solution is smooth if we use impedance coupling conditions. In addition, the second order coupling scheme, as expected, appears more accurate at all range of density ratios. Since the motion of the piston is governed by Newton's second law it can be shown (Dunn, 2011) that it is described by equation

$$\frac{d^2x}{dt^2} = \frac{p_* A}{m_{sol}}\left[\left(\frac{V_*}{V_* + Ax}\right)^{\gamma} - \left(\frac{V_*}{V_* - Ax}\right)^{\gamma}\right], \tag{27}$$

where x is the center of mass of the piston, p_* and V_* are the pressure and volume at equilibrium, A is the frontal area of the piston equal to 1 here, m_{sol} is the mass of the piston. Figure 7b shows results of comparisons with the analytical solution. The second order coupling scheme with impedance coupling conditions match very well the analytical solution.

9.4 Modified Sod problem

To demonstrate that the proposed coupling technique is applicable and stable when both foreground and background solvers have similar properties the method has been applied to the Sod shock tube test case. The initial conditions are $(\rho, u, p)_L = (1, -0.5, 1)$, $(\rho, u, p)_R = (0.125, 0, 0.1)$, where the initial discontinuity is placed at x=0.5 and the foreground grid with gamma law gas was initially placed at x=0.6 (Figure 8a). The background domain of size 1x1 was discretized using 128x128 mesh resolution. The foreground domain of initial length 0.25 was discretized with 32x32 mesh resolution. Figure 8 shows the pressure, density and velocity profiles in both background and foreground regions. The foreground grid is allowed to move and it deforms and propagates with the shock wave. The pressure, density and velocity are similar on both meshes, but they are sharper for the foreground mesh since this mesh moves with the shock wave and have little numerical dissipation. In this example, the background and foreground solvers have similar properties (gamma law gases in this example). Therefore, this example demonstrates that the proposed coupling technique is stable and capable reproducing discontinuities at the interfaces between domains with similar material properties.

9.5 Shock wave interaction with Lagrange structure

This is a validation test of the multiphase model for a simulation of a shock wave impacting a steel panel. The test is designed to test fluid-structure interaction for a transient compressible flow. A two-dimensional planar geometry was used in the calculations. The problem dimensions are given in Figure 9a. A thin steel plate is placed at the center of a rectangular domain. An initial high-pressure, high temperature region (p=10^{1} Mbar, T=3000 K) of radius 10 cm is placed at x= 25 cm. The surrounding gas has atmospheric air conditions (p=1^{-6} Mbar, T=300 K). This initial pressure and temperature jump generates a shock, which impacts the panel and induces flexure of the plate. The thickness of the plate is 10 cm. The background mesh has resolution 50x50 cells. The steel panel (foreground mesh) is discretized using 5x25 cells. The plate is modeled using the Lagrangian structural model for steel while the air is modeled as a single-phase material using the multiphase method. No analytic solution is available for this test. Therefore, we compare results of the simulations with conforming grid simulations that are done with the same initial conditions and resolution. In the last case, the conforming grid stretches and deforms as the plate moves whereas in the first case the background mesh remains uniform. Figure 9 shows snapshots of velocity field in both simulations at time 0.2 s (embedded approach – Figure 9c, conforming grid – Figure 9d) and 0.65 s (embedded approach – Figure 9e, conforming grid – Figure 9f). Figure 9b shows comparison of the averaged velocity in the plate in both simulations. We see that results obtained using two different techniques agree very well. Therefore, we conclude that the multiphase-flow algorithm appears to be coupled to the Lagrangian structure properly for this problem.

9.6 Shock wave with tungsten particles interaction with Lagrange structure

This last example demonstrates interaction of a shock wave that consists of tungsten particles with a solid structure. The setup is similar to the previous example but now the initial high-pressure region consists of tungsten particles (10% volume fractions) and air (90% volume fraction). Figure 9 shows reflection of the tungsten particles from the structure once they interact with a plate. Several drag models are available to parametrize air-particles coupling terms. For

this particular simulation, we used Akhatov drag model (Akhatov and Vainshtein 1984). The background mesh has resolution 120x120x120 cells. The steel target (foreground mesh) is discretized using 40x40x10 cells. As flow with the tungsten particles reaches the target, the steel panel starts to deform and solid stresses inside the steel target are developed (Figure 10). These results demonstrate that the coupling algorithms used in the current approach are appropriate for modeling the interaction between multiphase particles and Lagrange structures.

10. Conclusions

A numerical technique to couple an Eulerian multiphase flow solver with Lagrangian hydrodynamics has been developed. The primary purpose is to allow simulations using different solvers operating on different domains and meshes. A number of algorithmic ideas are combined to design a coupling technique in such a way that coupling occurs only through interfaces, allowing simulation codes to remain separate. Some unique features of this work included development of multiphase interface conditions that are appropriate for the multi-phase flow conditions across the entire range of material parameters. In addition to the cell centered updates in ghost points similar to the ghost fluid methods we use additional modifications of the solid states at the faces in such a way that resulting solution of the Riemann problem at the faces satisfies the boundary interface conditions and approves accuracy of the scheme. The ability of the new coupling technique to reproduce complex features of the interaction of multiphase flow with Lagrange structures is presented on several examples. These examples demonstrate the efficiency and potential of the present technique to simulate interaction of the multiphase blast with deformable tragets.

Acknowledgment

This work was performed under the auspices of the US Department of Energy by Lawrence Livermore National Laboratory under Contract DE-ASC52-07NA27344. The work is supported in part by the Joint DoD/DOE Munitions Technology Development Program. We also greatly acknowledge the NNSA ASC Program for supporting this research.

References

1. Akhatov, I. S. & Vainshtein, P. B. 1984 Transition of porous explosive combustion into detonation. *Combustion Explosion And Shock Waves* **20** (1), 63–69.
2. Banks, J. W., Sjogreen, B. A normal mode stability analysis of numerical interface conditions for fluid/structure interaction. *Comm. In Comp. Physics*, **10**(2):279-304, 2011
3. Banks, J. W., Henshaw, W. D. , Schwendeman, D. W., An analysis of a new stable partitioned algorithm for FSI problems. Part I: Incompressible flow and elastic solids, *J. of Comp. Physics*, 269:108–137, 2014.
4. Chinnayya A., E. Daniel, and R. Saurel. 2004. Modelling detonation waves in heterogeneous energetic materials. Journal of Computational Physics, 196(2):490–538.
5. Dunn, T.A. "A cell-centered multiphase ALE scheme with structural coupling", Ph.D. dissertation, University of California, Davis, 2011.
6. Fedkiw, R. P. Coupling an Eulerian fluid calculation to a Lagrangian solid calculation with the ghost fluid method. *J. of Comp. Physics*, **175**:200-224, 2002.
7. Ghias R., Mittal R., Dong H. A sharp interface immersed boundary method for compressible viscous flows. *J. of Comp. Physics,* **2225:** 528-553, 2007.
8. Gorsse, Y., Iollo A., Telib, H., Weynans, L. A simple second order Cartesian scheme for compressible Euler flows. *J. of Comp. Physics,* **231:** 7780-7794, 2012.
9. Noble et al., 2017. ALE3D: An Arbitrary Lagrangian-Eulerian Multi-Physics Code. Technical Report, Lawrence Livermore National Laborartory, LLNL-TR—732040
10. Pember R. B., Bell J. B., Colella P., Crutchfield W. Y., Welcome M. L. An adaptive Cartesian grid method for unsteady compressible flow in irregular regions. *J. Comput. Phys* 120, 1995, 278–304
11. Peskin C. S. The immersed boundary method *Acta Numerica*, 11, 2002, 479-517.
12. Puso, M., Sanders, J., Settgast, R. and Liu, B., "An embedded mesh method in a multiple material ALE," *Computer Methods in Applied Mechanics and Engineering*, 245, 273-289 (2012).
13. R. Saurel and R. Abgrall. A multiphase godunov method for compressible multifluid and multiphase flows. *J. of Comp. Physics*, 150(2):425–467, 1999.

14. M. Sun and K. Takayama. An artificially upstream flux vector splitting scheme for the Euler equations. J. *of Comp*. *Physics*, 189(1):305–329, July 2003.
15. Thornber B., D. Drikakis, R.J.R. Williams, D. Youngs. On entropy generation and dissipation of kinetic energy in high-resolution shock-capturing schemes. J. Comp. Phys., 227 (2008), 4853-4872.
16. Thornber B., A. Mosedale, D. Drikakis, D. Youngs, R.J.R. Williams. An improved reconstruction method for compressible flows with low Mach number features. J. Comp. Phys., 227 (2008), 4873-4894
17. Tipton D. G., M. A. Christon, M. S. Ingber. Coupled fluid-solid interaction under shock wave loading. Int. J. For Numer. Methods in Fluids, 67, 2011, 848-884.
18. Venkateswaran, S., Merkle, C.L., 1998. Evaluation of artificial dissipation models and their relationship to the accuracy of Euler and Navier–Stokes computations. In: Lecture Notes in Physics. 16th Int. Conf. on Numer. Methods in Comp. Physics, vol. 4(12). pp. 427–432.

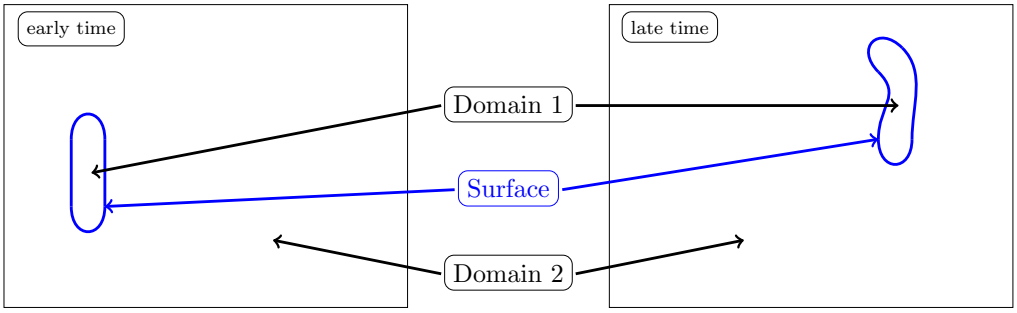

Figure 1. A cartoon depicting the evolution of a multi-domain problem.

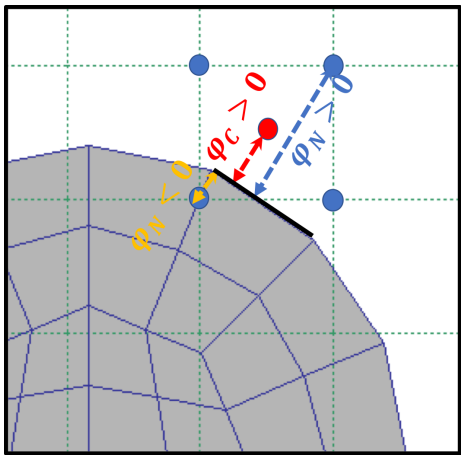

Figure 2. An example of signed distances evaluation for the nodes and the cell center.

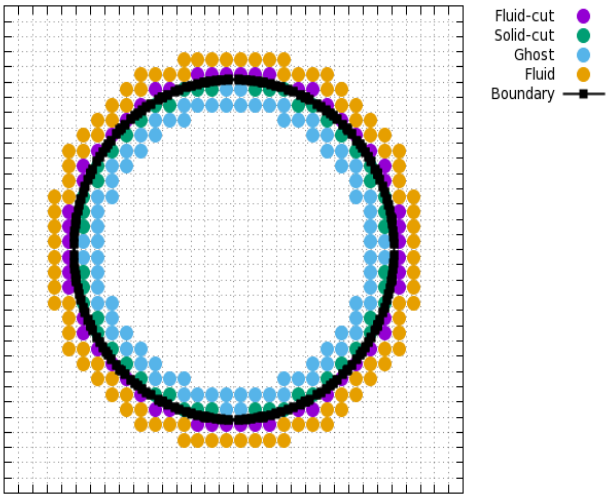

Figure 3. An example of circular foreground Lagrangian boundary and the background mesh element categories that participate in coupling.

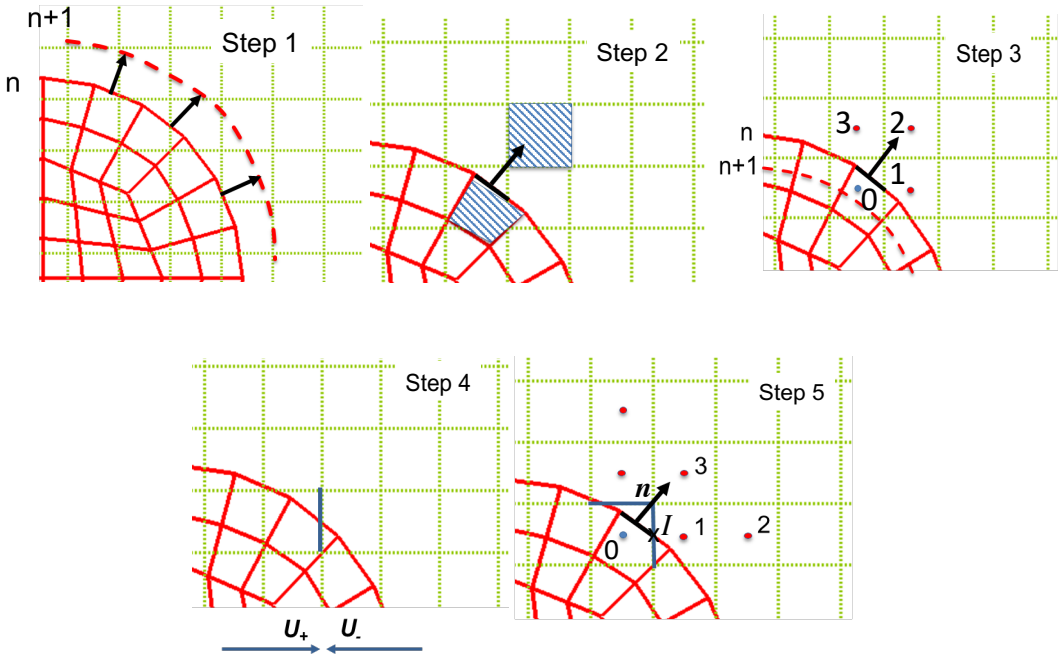

Figure 4. Illustration of the multi-step coupling algorithm for the multiphase solver operated on the background grid (green) and Lagrange hydro operated on the foreground grid (red).

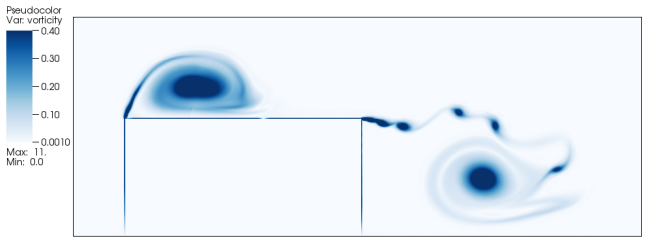

(a)

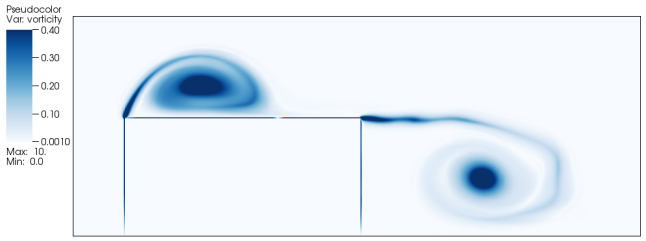

(b)

Figure 5. Results of the interaction of subsonic flow with a step solid structure. The calculated voriticity using the modified low Mach scheme is shown in (a) and the standard compressible scheme results are shown in (b). The low Mach number features presented in (a) are heavily damped by the standard compressible numerical scheme (b).

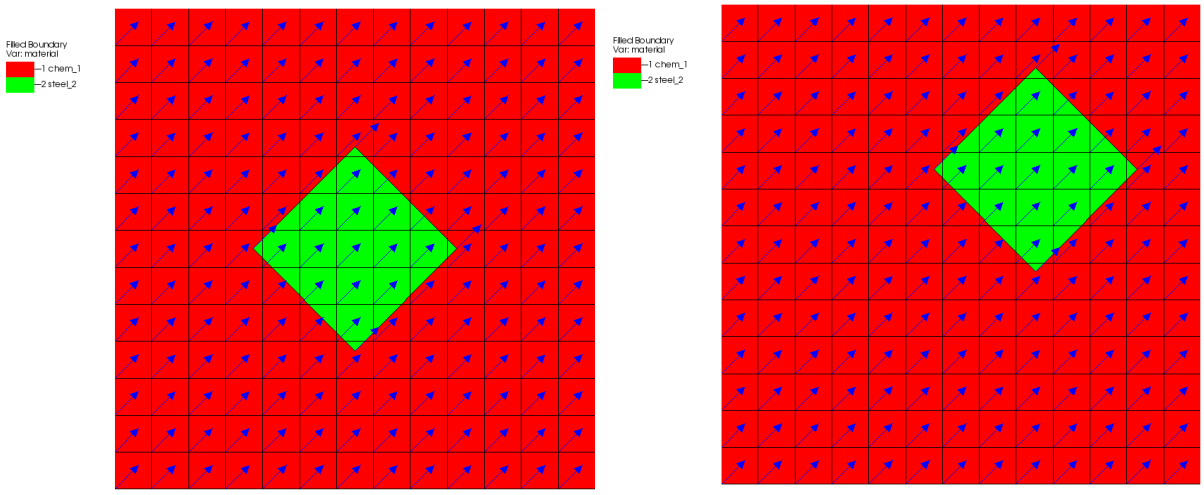

t=0 ms t=30 ms

Figure 6. Advection of the Lagrangian object moving with the matching velocity of the fluid. As expected, no artificial flows are generated. Therefore, the interface conditions are implemented correctly.

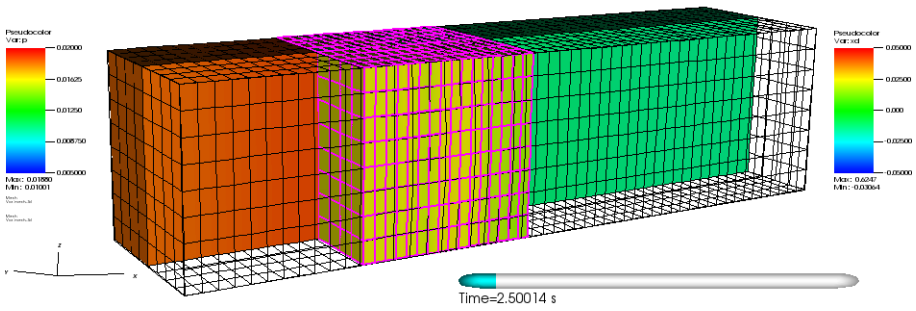

(a)

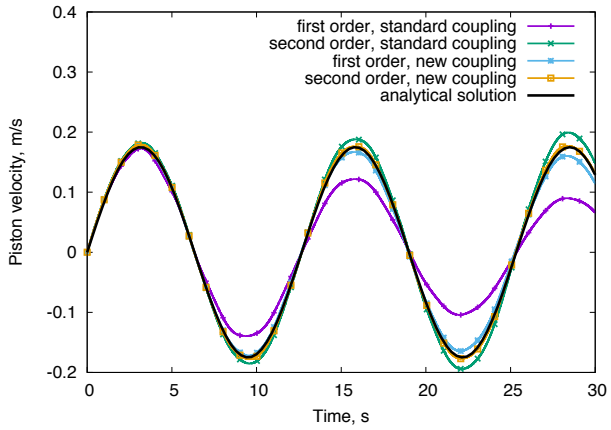

(b)

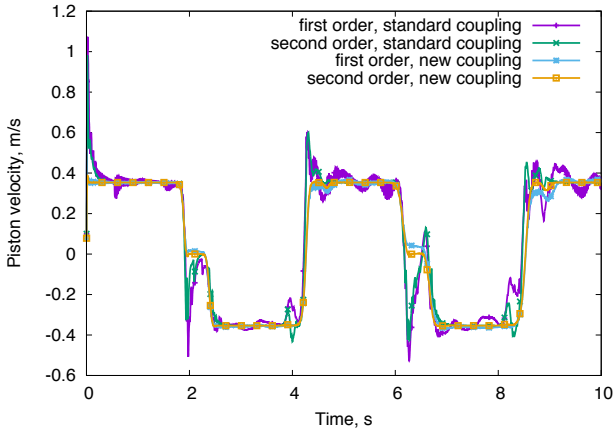

(c)

Figure 7. Pressure driven piston calculation showing the importance of numerical boundary and coupling methods at different solid/fluid density ratios. A high-pressure gas on the left pushes a solid piston to the right (a). The piston velocity is shown for solid/fluid density ratios of 100 along with the analytical solution (b) and solid/fluid density ratios of 0.01 (c). Without the impedance based interface conditions, spurious waves are generated.

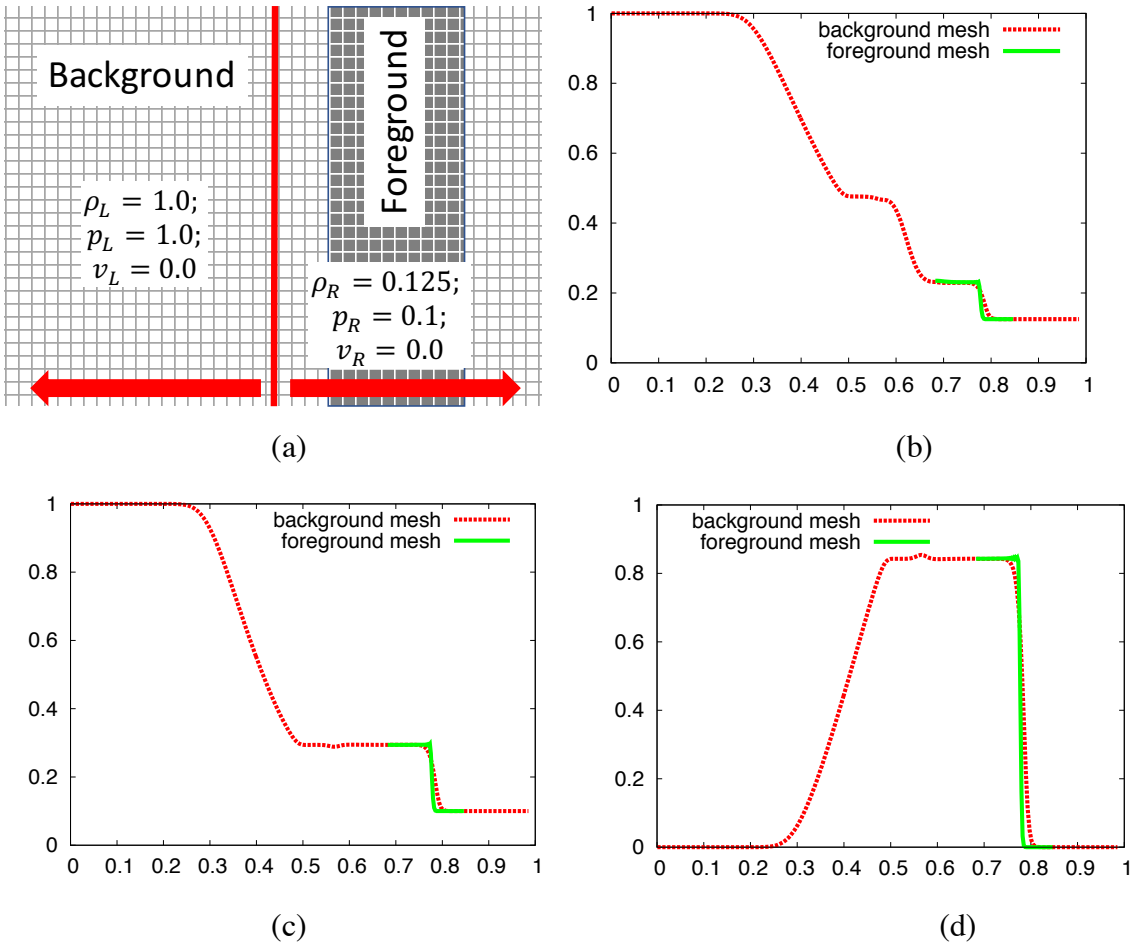

Figure 8. Results from the modified Sod shock tube test case problem for coupled meshes. A foreground mesh is initially placed at the right (a). Both background and foreground material is gamma-low air therefore impedance-averaged conditions are important in this example. As shock propagates to the right, foreground mesh moves. Density (b), pressure (c) and velocity (d) at time t=0.15 in both background solvers and foreground solvers are shown.

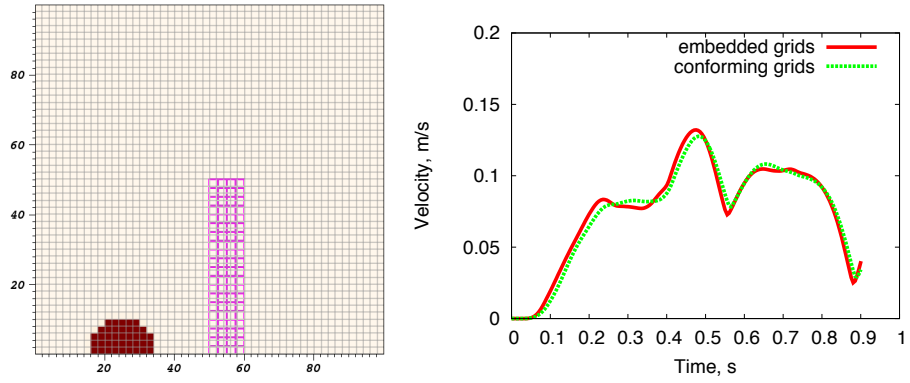

(a) (b)

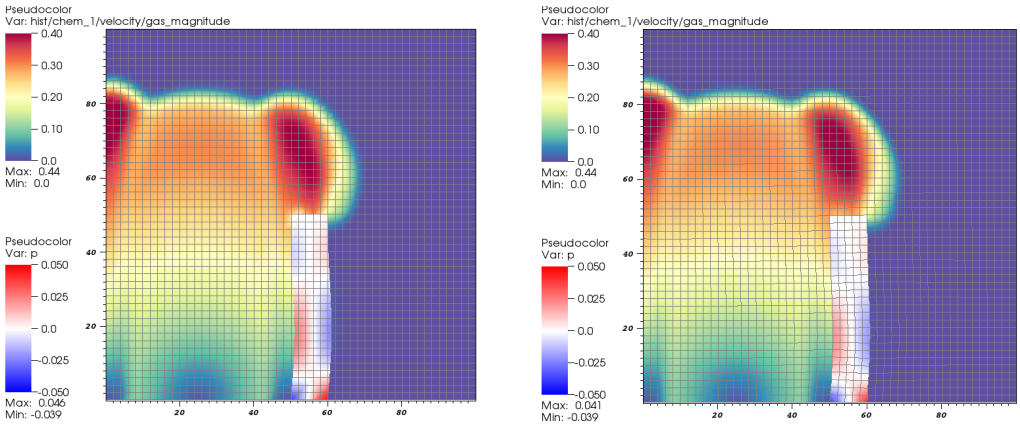

(c) (d)

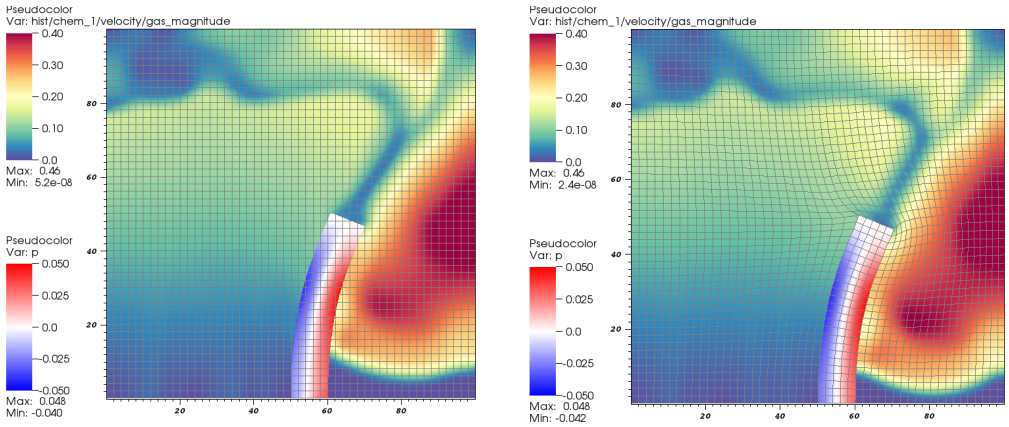

(e) (f)

Figure 9. Comparison of shock wave interaction with a Lagrange deformable structure. The initial pill of high-pressure air is located on the left (a). Simulations are done with the embedded grids method presented in this work and compared to a conformal mesh method. Velocity field comparison are presented for time 0.17 s (embedded grid (c) and conformal mesh –(d) and a time 0.67 s (embedded grid (e) and conforming mesh (f).

585

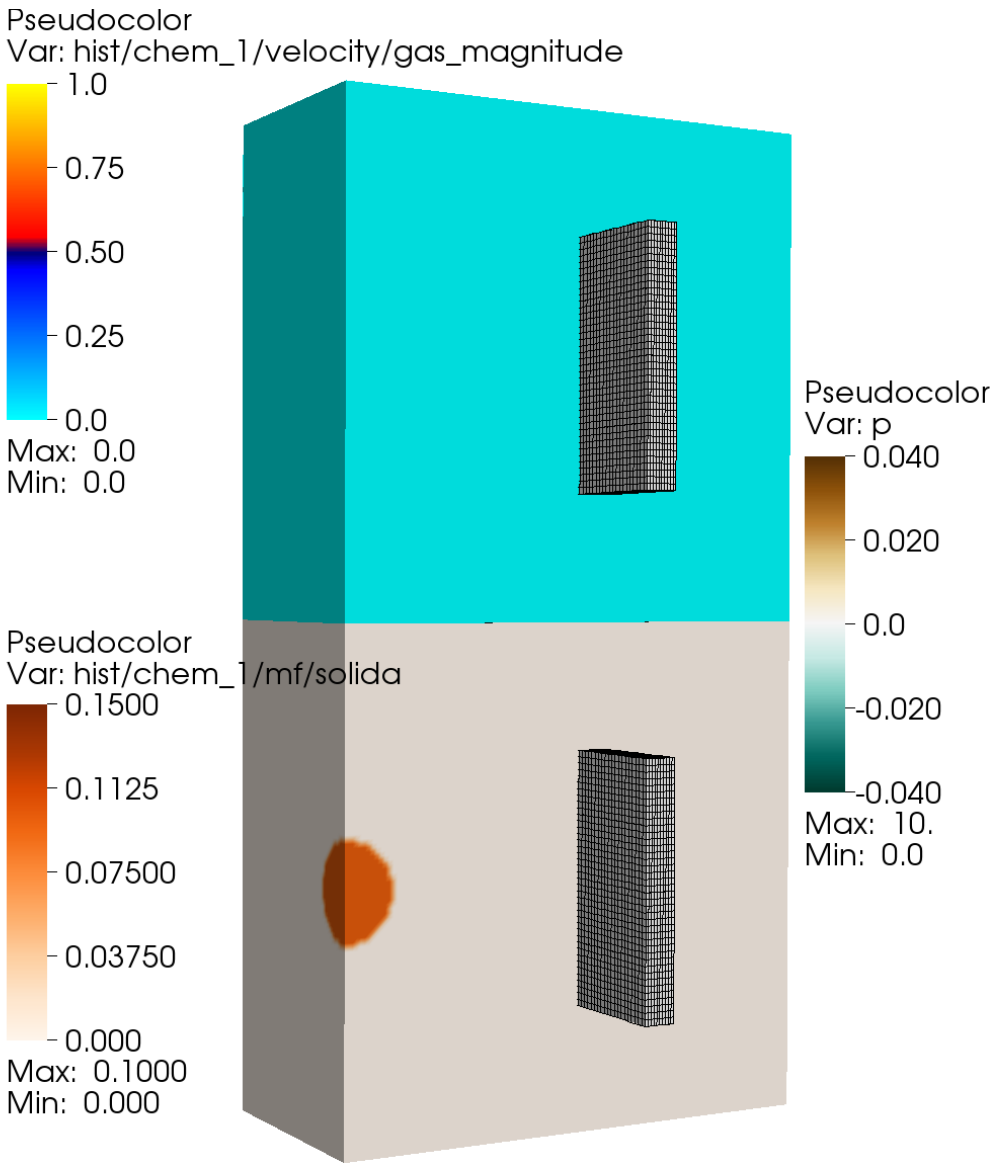

586

587 t = 0 ms

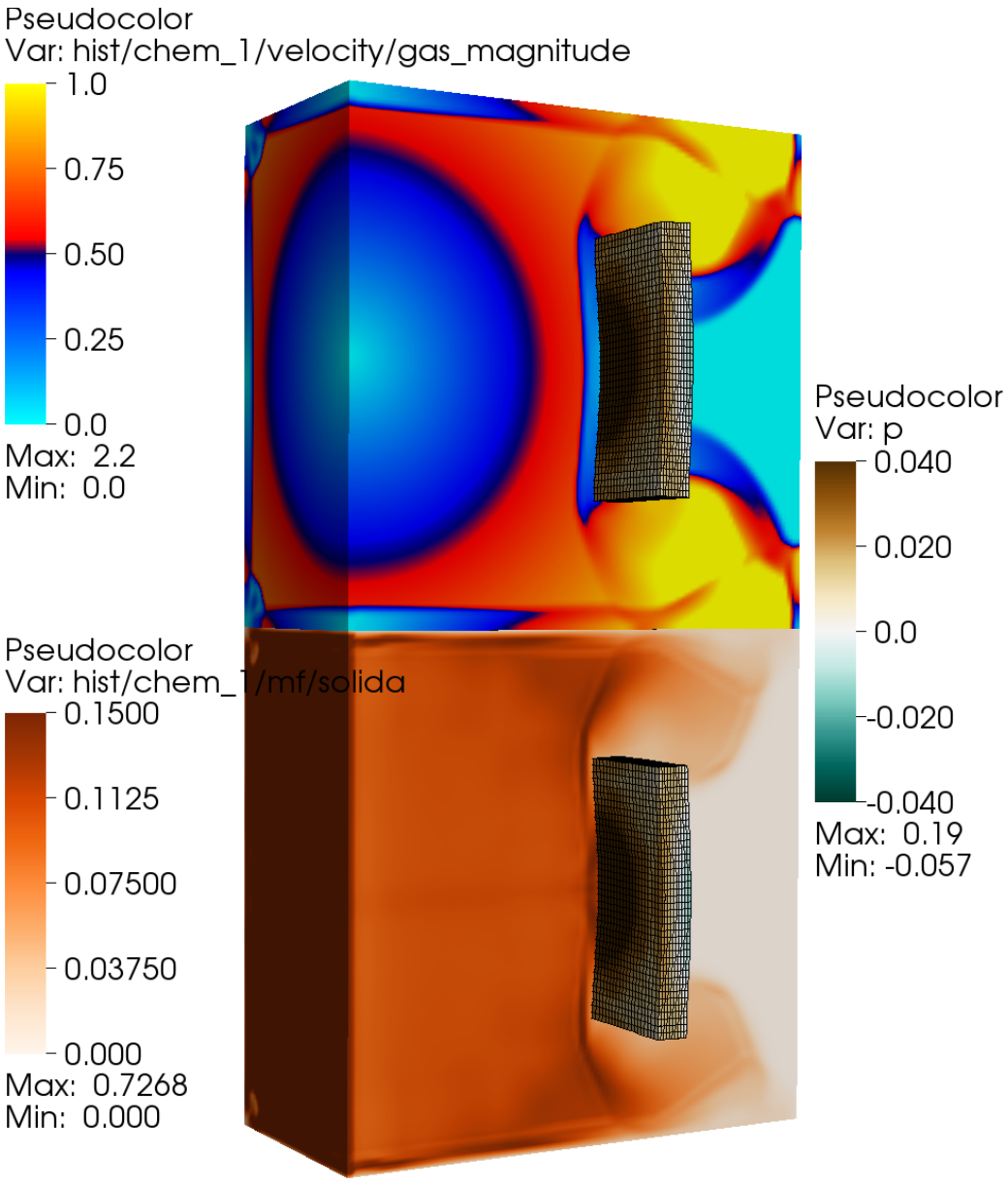

588

589 t = 100 ms

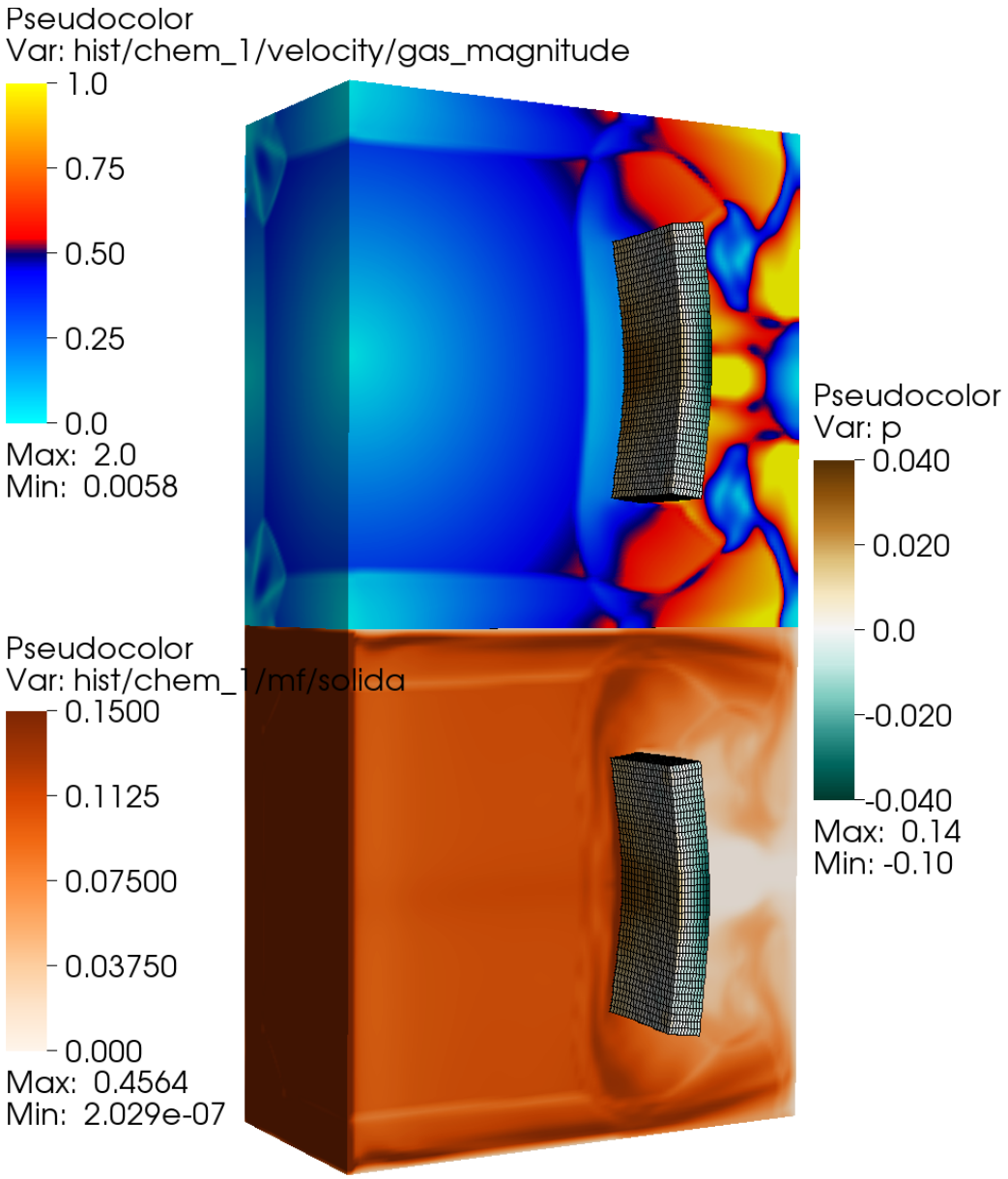

T=150 ms

Figure 10. A blast wave that consists of tungsten particles (10% volume fraction) and air (90% volume fraction) interacts with a solid structure. Once particles reach the wall they are reflected. The velocity field in the air phase is shown in the upper panels and the particle mass fraction is shown in the lower panels. Also shown are stresses developed inside the steel plate due to the interaction with the shock wave.